Smart Structures and Systems, *Vol. 35, No. 6 (2025) 327-336*
https://doi.org/10.12989/sss.2025.35.6.327

A self-powered magnet-less tunable piezoelectric vibration sensor based on stress distribution

Mehdi Aslinezhad [1a], Sajad Hadidi*[2] and Alireza Malekijavan [1b]

[1] *Department of Electrical Engineering, Shahid Sattari Aeronautical University of Science and Technology, 1384663113, Tehran, Iran*
[2] *Faculty of Electrical Engineering, Shahid Beheshti University, 1983969411, Tehran, Iran*

(*Received November 13, 2024, Revised February 28, 2025, Accepted June 30, 2025*)

Abstract. This paper presents a self-powered tunable piezoelectric vibration sensor based on stress distribution. The piezoelectric sensor features split electrodes to adjust the resonance frequency. Turning electrically OFF configurable electrodes changes the sensor stiffness by varying the stress level. Unlike previous works, the proposed tunable sensor does not use a magnet or an auxiliary mass. The effect of the tuning mechanism on the resonance frequency, voltage sensitivity, and power density has been investigated through theoretical analysis, simulation, and experimentation. The paper explores the effect of the stress level on sensor linearity. The paper also examines the impact of thickness and length on the frequency tuning range. The tuning mechanism achieves a tuning range of 8.6 Hz with a thickness ratio of 0.2 and a length of 90 mm, surpassing the capabilities of most fine-tuning mechanisms. The tunable sensor has a good linearity of $R^2 \approx 0.98$. Within 116.9 Hz to 120.8 Hz, the minimum power density is 100 μW/cm^3 for a 1 g input excitation level. In mode 100, the sensor voltage sensitivity and power density increase by about 83% and 11%, respectively, compared to a conventional sensor. The self-powered tunable piezoelectric vibration sensor can compensate for physical uncertainty, such as inherent variability in material properties and manufacturing tolerances.

Keywords: configurable electrodes; piezoelectric material; self-powered; stress distribution; tunable; vibration sensor

1. Introduction

The Internet of Things (IoT) market is developing with rapidly increasing active IoT devices (Majumder *et al*. 2018, Khosravani and Reinicke 2020, Rehman *et al*. 2024, Mamun and Yuce 2019, Li *et al*. 2020, Rigo *et al*. 2024). Powering IoT devices will be a big challenge shortly. Green and self-powered IoT needs to eliminate disposable batteries. While most available vibration sources are found at frequencies below 200 Hz, self-powered vibration sensors show promise as a solution for wireless sensor nodes (Roundy *et al*. 2003). Electromechanical transducers such as piezoelectric (Li and Lee 2022, Liang *et al*. 2021, Habib *et al*. 2022, Trentadu *et al*. 2019, Mishra *et al*. 2020), electromagnetic (Muscat *et al*. 2022), and electrostatic (Yan *et al*. 2021) act as self-powered vibration sensors. Electromechanical transducers convert vibration to electrical energy, and simultaneously, the output of the transducer is the readout of an event of interest. The piezoelectric transducers are low-cost, small-size, no-heat generation electromechanical transducers (Shirvanimoghaddam *et al*. 2019, Pecunia *et al*. 2023, Hadidi and Hassanzadeh 2023).

Piezoelectric transducers use the direct piezoelectric effect to convert vibration to electric charges or an AC voltage. Eq. (1) describes the direct piezoelectric effect

$$D = dT + \varepsilon E \tag{1}$$

D is the electric displacement, T and E are the stress and electric field, and d and ε are the direct piezoelectric coefficient and permittivity (Covaci and Gontean 2020).

Piezoelectric transducers suffer from narrow bands, low power density, and physical uncertainty, such as inherent variability in material properties and manufacturing tolerances, which impact the resonance frequency. Recent studies have focused on developing frequency-tuning techniques and exploring the tuning effects on power density (Liu *et al*. 2023, Yoon and Youn 2018, Qin *et al*. 2019). The literature primarily concentrates on tuning techniques for vibration piezoelectric energy harvesters to maximize output power. Both the piezoelectric energy harvester and the self-powered piezoelectric sensor exploit the direct piezoelectric effect. Specifically, the piezoelectric sensor measures vibration, and the sensor's output serves as the readout of an event. Researchers have adjusted the mass and stiffness of piezoelectric transducers to tune their resonance frequency. Huet *et al*. (2022) have developed a tunable piezoelectric harvester for wireless sensor nodes (WSN) to adapt the piezoelectric transducer to the vibration source. The coarse tuning is achieved by the mass weight, and fine-tuning by mobile clamping. Using a tip mass of 3.9 grams, moving the clamp position changes the resonance frequency from 100.8 Hz to 123.1 Hz. In the tuning range,

*Corresponding author, Ph.D.,
E-mail: s_hadidi@sbu.ac.ir
[a] Assistant Professor
[b] Associate Professor

ISSN: 1738-1584 (Print), 1738-1991 (Online)

the power density sharply decreases from 406 μW/cm^3 for an optimal load resistance of 31 kΩ to 19 μW/cm^3 with an optimal load resistance of 26 kΩ, under an input acceleration of 0.5 g (g = 9.8 m/s^2). Dong *et al*. (2022) have proposed an enhanced piezoelectric harvester based on a dual-mass configuration for track vibration. The dual-mass configuration uses a typical tip mass and an additional middle mass to change the resonance frequency. The position of the middle mass is used for fine-tuning, and the mass weight to coarse adjustment. The middle mass position adjusts the resonance frequency from 720 Hz to 725 Hz, increasing the power density by 32%. Wang *et al*. (2021) have introduced an intelligent piezoelectric vibration energy harvesting device to achieve frequency self-tracking. The moving of a sliding mass on the longitudinal holes of a cantilever beam fine-tunes the resonance frequency from 6 Hz to 9 Hz. In the adjustment range, the power density reduces from 33 mW/cm^2 to 14.4 mW/cm^2 for a 1.3 g acceleration level. Shi *et al*. (2021) have presented a vibration energy harvester based on zigzag piezoelectric springs actuated by a rolling ball. The spring length and the ball weight adjust the natural frequency from 2.3 Hz to 4.7 Hz and 1.5 Hz to 3 Hz, respectively. In the 1 Hz to 4 Hz range, the maximum power density is 7.5 μW/cm^3 for a load resistance value of 5.1 kΩ. Sosna *et al*. (2023) have proposed a tunable vibration energy harvester using two magnets. The magnetic gap between magnets creates a nonlinear magnetic stiffness that tunes the frequency response from 20 Hz to 65 Hz by adjusting the magnet separation from 9 mm to 1 mm. In the tuning range, the power density decreases from 0.56 mW/cm^3 to 0.26 mW/cm^3 for an optimal load resistance of 76 kΩ and an input acceleration of 0.5 g. Ganapathy *et al*. (2021) have introduced a hybrid energy harvester based on the piezoelectric effect that uses a triboelectric layer and two magnets. The triboelectric surface area alters the effective mass, and magnets change stiffness. Increasing the surface area from 3 cm^2 to 9 cm^2 reduces the resonance frequency from 52 Hz to 50 Hz. The 1.5X magnetic stiffness reduces the resonance frequency from 54 Hz to 38 Hz. The maximum output power is 659 μW at 44 Hz at 180 kΩ, and the minimum at 54 Hz is about 350 μW. Le Scornec *et al*. (2020) have investigated the effect of the mass position on a piezoelectric energy harvester performance. The distance between mass and clamp, from 7.5 cm to 4 cm, changes the resonance frequency from 9.9 Hz to 16 Hz. Tuning the resonance frequency reduces the maximum extracted power from 127 μW to 72 μW for a constant acceleration of 1 g at an optimal load resistance of about 250 MΩ.

Using multi-electrodes instead of a monolithic electrode realizes a tunable piezoelectric transducer (Stewart *et al*. 2012). Hadidi and Hassanzadeh (2024) have presented an electrode-based method to maximize the output power of a piezoelectric vibration energy harvester. Due to charge redistribution in piezoelectric transducer, halving the electrode length maximizes the extracted power.

In this paper, configurable electrodes tune the resonance frequency of a piezoelectric vibration sensor. The proposed technique can improve the sensor voltage sensitivity and power density. The paper is structured as follows. In section 2, the sensor principle is described. Section 3 proposes a novel tunable piezoelectric vibration sensor and theoretically analyzes the effects of the tuning mechanism on the resonance frequency, linearity, voltage sensitivity, and output power. A connection configuration circuit is proposed for controlling the electrodes in section 3.4. Section 4 studies simulation and experimental results and compares the proposed sensor with previous works. The last section presents the paper conclusion.

2. Sensor principle

Fig. 1(a) shows a piezoelectric vibration sensor consisting of a substrate, a piezoelectric layer, and monolithic electrodes. Fig. 1(b) illustrates a mechanical model of the vibration sensor, in which M and K are the mass and stiffness, and c is the damping coefficient. The piezoelectric sensor uses the direct piezoelectric effect, converting vibration to an output voltage. According to the Hamilton principle, motion equations for the piezoelectric vibration sensor are as follows (Xu and Tang 2015, Lee and Moon 1990)

$$M\ddot{q} + c\dot{q} + Kq + k_1 v = F \tag{2a}$$

$$C_p\dot{v} + \frac{v}{R_L} + k_1\dot{q} = 0 \tag{2b}$$

q and v represent the sensor displacement and output voltage. R_L and C_p denote the load resistance and piezoelectric capacitance across the electrodes. k_1 indicates the electromechanical coupling term. F is the excitation force. The voltage amplitude ($\tilde{V}$) is obtained by solving Eq. (2)

$$\tilde{V} = \frac{Mr\Omega k_e \tilde{F} i}{C_p\left((r\Omega i + 1)(-\Omega^2 + \varsigma\Omega i + 1) - k_e^2\right)} \tag{3a}$$

$$\omega_n = \frac{A_n}{l^2}\sqrt{\frac{K}{M}}, \Omega = \frac{\omega}{\omega_n}, \varsigma = \frac{c}{\sqrt{KM}} \tag{3b}$$

$$r = R_L C_p \omega_n, k_e^2 = C_p\frac{k_1^2}{K} \tag{3c}$$

$\tilde{F}$ indicates the force amplitude. ω_n, Ω, and ς represent the natural frequency, dimensionless excitation frequency, and mechanical damping ratio. A_n is the constant proportional to the nth natural frequency. l is the cantilever length. r and k_e denote non-dimensional load resistance and electromechanical coupling coefficient.

3. Proposed tunable piezoelectric vibration sensor

The self-powered tunable piezoelectric vibration sensor based on stress distribution is shown in Fig. 2(a). The tunable sensor consists of a substrate, a piezoelectric layer, and multiple electrodes coated on the piezoelectric layer.

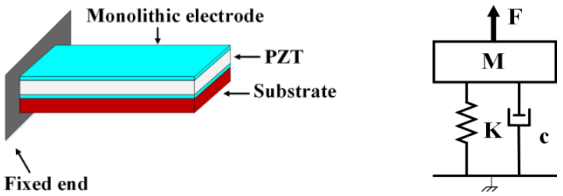

(a) (b)

Fig. 1 (a) Conventional piezoelectric vibration sensor; (b) Mechanical model

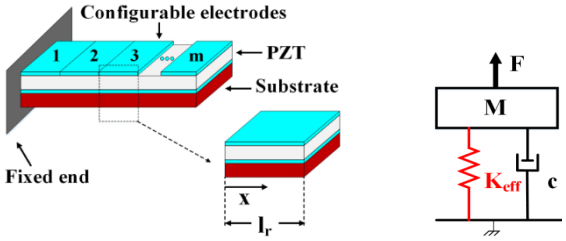

(a) (b)

Fig. 2 (a) Tunable piezoelectric vibration sensor; (b) Mechanical model

The sensor's frequency response is adjusted by turning electrically OFF configurable electrodes, as the electrodes experience varying stress levels in different positions. The stress level diminishes along the beam's length, from the fixed end to the free end of the cantilever beam, and maximum stress occurs when all electrodes are activated.The stress level changes the effective stiffness (K_{eff}) shown in the mechanical model in Fig. 2(b). Altering the stiffness tunes the natural frequency of the vibration sensor as follows (Erturk and Inman 2008, ANSI/IEEE Std 176-1987 1987)

$$f_n = \frac{A_n}{2\pi l^2}\sqrt{\frac{K}{M}} = \frac{A_n}{2\pi l^2}\sqrt{\frac{K_s + K_p}{M}} = \frac{A_n}{2\pi l^2}\sqrt{\frac{Y_s I_s + Y_p I_p}{M}} \quad (4)$$

Y and I represent Young's modulus and moment of inertia. Y_sI_s and Y_pI_p denote the substrate bending stiffness and piezoelectric bending stiffness, in which the piezoelectric Young's modulus is

$$Y_p = (s_{11}^E - d_{31}g_{31})^{-1} \quad (5a)$$

$$g_{31} = d_{31}\frac{bl}{hC_p} \quad (5b)$$

s_{11}^E is the elastic compliance component. d_{31} and g_{31} represent the piezoelectric charge constant and piezoelectric voltage constant. The b, l, and h indicate the piezoelectric layer width, length, and thickness. C_p is the piezoelectric capacitance.

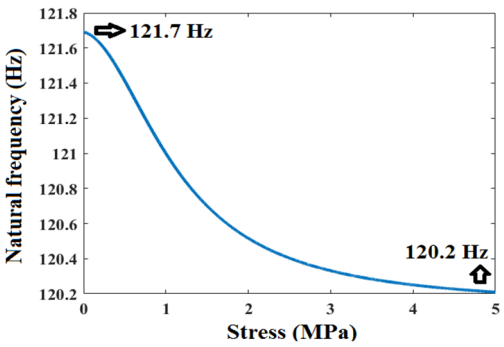

Fig. 3 Stress effect on the natural frequency

The elastic compliance component and piezoelectric constants are defined in Eq. (6) for low stress levels (Meeks and Timme 1975, Gusarov *et al*. 2016).

$$s_{11}^E = s_{11}^E|_{\Delta T=0} + \alpha T + \beta T^2 = s_{11}^E(0) + \gamma(T) \quad (6a)$$

$$g_{31} = g_{31}|_{\Delta T=0} + \alpha T + \beta T^2 = g_{31}(0) + \gamma(T) \quad (6b)$$

$$d_{31} = d_{31}|_{\Delta T=0} + \alpha T + \beta T^2 = d_{31}(0) + \gamma(T) \quad (6c)$$

$\gamma(T) = \alpha T + \beta T^2$. T represents the stress level. α and β are constant coefficients and can be determined by the Rayleigh law (Damjanovic and Demartin 1996). According to Eqs. (4)-(6), the effective natural frequency can be rewritten as

$$f_{n,eff}(T) = \frac{A_n}{2\pi l^2}\sqrt{\frac{K_{eff}}{M}} = \frac{A_n\left[Y_sI_s + \left((s_{11}^E(0)+\gamma) - (g_{31}(0)+\gamma)(d_{31}(0)+\gamma)\right)^{-1}I_p\right]^{\frac{1}{2}}}{2\pi l^2 M^{\frac{1}{2}}} \quad (7)$$

Fig. 3 shows the effect of the stress level on the natural frequency. Increasing the stress level from 0 to 5 MPa changes the natural frequency by about 1.5 Hz. Therefore, configurable electrodes change the stress level to adjust the effective natural frequency expressed in Eq. (7). The frequency tuning range (FTR) of the proposed sensor is defined in Eq. (8)

$$FTR = f_n(max)|_{T=min} - f_n(min)|_{T=max} \quad (8)$$

The stress level and natural frequency have an inverse relationship: minimum stress results in maximum natural frequency, while maximum stress leads to minimum natural frequency. The following sections explore how turning the electrodes off affects sensor linearity, voltage sensitivity, and output power.

3.1 Sensor linearity

This section analyzes the stress effect on the linearity of a segmented beam with electrodes. Using the Bubnov–Galerkin method, the beam defection, $w(x, t)$, is expressed as a summation of eigenfunctions, which involves the products of generalized displacements, $q_r(t)$, with the corresponding orthogonal basis functions, $\varphi_r(x)$ (Patel *et al*. 2014, Shahabi *et al*. 2019)

$$w(x,t) = \sum_{r=0}^{m} \varphi_r(x)\, q_r(t) \tag{9}$$

The nonlinear equation of the beam motion near the fundamental frequency is

$$M\ddot{q} + c\dot{q} + Kq + K_1 q^3 + K_2 q^5 = F \tag{10a}$$

$$K_1 = \lambda_1 \int_0^l \varphi[\ddot{\varphi}^2 \dddot{\varphi} + 2\ddot{\varphi}\dddot{\varphi}^2]\, dx \tag{10b}$$

$$K_2 = \lambda_2 \int_0^l \varphi[6\ddot{\varphi}^3 \dddot{\varphi}^2 + \ddot{\varphi}^4 \dddot{\varphi}]\, dx \tag{10c}$$

K_1 and K_2 are nonlinear coefficients. λ_1 and λ_2 achieve a constant magnitude in the steady-state vibration of the sensor. l is the beam length. The beam function for the r^{th} section's motion of the segmented beam is

$$\begin{aligned}\varphi_r(x) = a\, sin\left(\frac{\delta_r x}{l_r}\right) + b\, cos\left(\frac{\delta_r x}{l_r}\right) \\ + c\, sinh\left(\frac{\delta_r x}{l_r}\right) + d\, cosh\left(\frac{\delta_r x}{l_r}\right)\end{aligned} \tag{11}$$

a, b, c, and d represent constants determined using boundary conditions. x denotes the distance from the left side of the electrode, and l_r is the electrode length. δ_r can be defined as

$$\delta_r = (\omega_n)^{\frac{1}{2}} l_r \left(\frac{\rho_r A_r}{Y_r I_r}\right)^{\frac{1}{4}} \tag{12}$$

Y_rI_r, A_r, and ρ_r are the bending stiffness, cross-sectional area, and mass density of the r^{th} section of the segmented beam. By substituting Eqs. (5)-(6) into Eq. (12) and assuming $l_r = l$

$$\delta(T) = \frac{(\omega_n)^{\frac{1}{2}} l \left(\rho_s A_s + \rho_p A_p\right)^{\frac{1}{4}}}{\left[Y_s I_s + \left((s_{11}^E(0) + \gamma) - (g_{31}(0) + \gamma)(d_{31}(0) + \gamma)\right)^{-1} I_p\right]^{\frac{1}{4}}} \tag{13}$$

Fig. 4 depicts the relationship between δ and stress level. Decreasing the stress level negligibly reduces δ from 2.856 to 2.839 by about 0.017, as shown in Fig. 4. Even though turning OFF electrodes decreases the stress level, it slightly decreases nonlinear coefficients (K_1 and K_2) as described in Eq. (10). Therefore, the tuning mechanism preserves the sensor linearity.

3.2 Voltage sensitivity

In the proposed multi-electrodes piezoelectric sensor, the generated charge across the r^{th} electrode is expressed in Eq. (14) (Stewart *et al.* 2012, Hadidi and Hassanzadeh 2024, Du *et al.* 2017).

$$Q_r = \int_{X_{r-1}}^{X_r} -hbd_{31} \frac{\tilde{F}\, sin(\omega_0 t)}{I} \left(\frac{1}{2l}x^2 - x + \frac{1}{2}l\right) dx \tag{14a}$$

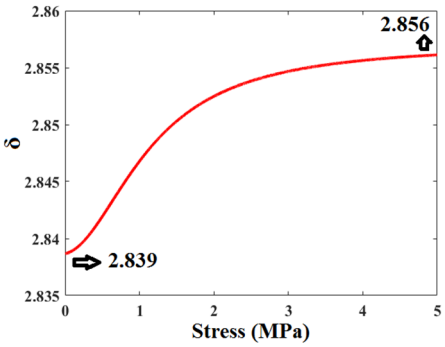

Fig. 4 Stress effect on δ

$$I = \frac{b(h+H)^3}{12} \tag{14b}$$

$l_r = X_r - X_{r\text{-}1}$ is the r^{th} electrode length. $\tilde{F}$ and ω_0 are the amplitude and angular frequency of the excitation force. I represents the second moment of area. l, b, and h are the piezoelectric length, width, and thickness. H is the substrate thickness. Therefore, the piezoelectric current of the r^{th} electrode (I_r) is

$$\begin{aligned} I_r &= \frac{dQ_r}{dt} = I_{0r}\, cos(\omega_0 t) \\ &= \omega_0 \int_{X_{r-1}}^{X_r} -hbd_{31} \frac{\tilde{F}}{I}\left(\frac{1}{2l}x^2 - x + \frac{1}{2}l\right) dx\, cos(\omega_0 t) \end{aligned} \tag{15a}$$

$$I_{0r} = -hbd_{31} \frac{\tilde{F}\omega_0}{I} \int_{X_{r-1}}^{X_r} \left(\frac{1}{2l}x^2 - x + \frac{1}{2}l\right) dx \tag{15b}$$

So, the voltage across the r^{th} electrode (V_r) is

$$V_r = \left(Z_r \parallel R_{L-opt.}\right) I_{0r} \tag{16a}$$

$$Z_r = R_r \parallel \frac{1}{\omega_0 C_{pr}} = \rho \frac{h}{bl_r} \parallel \frac{h}{\omega_0 \varepsilon b l_r} \tag{16b}$$

$$R_{L-opt} \approx \frac{1}{\omega_0 C_{pt}} \tag{16c}$$

ε is the permittivity. ρ represents the electrical resistivity of piezoelectric material. $R_{L\text{-}Opt}$ is the optimal load resistance. C_{pr} denotes the piezoelectric capacitance across the r^{th} electrode, and C_{pt} represents the equivalent piezoelectric capacitance. Eq. (16c) indicates changing the equivalent piezoelectric capacitance by turning off electrodes alters the optimal load resistance.

3.3 Output power

Considering Eqs. (15)-(16), the power generated by the piezoelectric transducer covered by the r^{th} electrode is

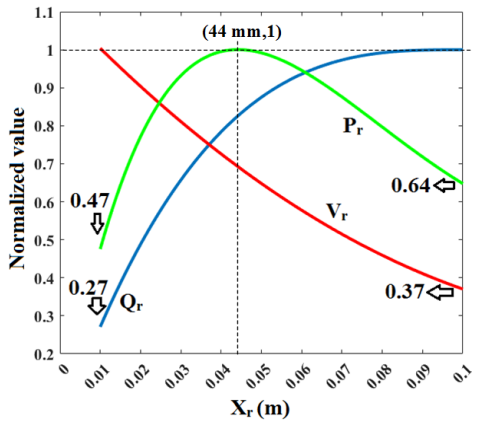

Fig. 5 Effect of the electrode position on the normalized generated charge, voltage, and power

(Stewart *et al*. 2012, Hadidi and Hassanzadeh 2024, Du *et al*. 2017)

$$P_r = \frac{1}{2}\left(Z_r \parallel R_{L-opt}\right) I_{0r}^2 \tag{17}$$

According to Eqs. (14)-(17), Fig. 5 shows the impact of the electrode position (X_r) on the normalized generated charge, voltage, and power when $X_{r\text{-}1}$ = 0 and l_r(min) = 10 mm. Considering $Q = d_{31}T$, the generated charge close to the free end is small due to the low-stress level. The maximum charge occurs in the monolithic electrode ($X_{r\text{-}1}$ = 0 and X_r = 100 mm). Turning OFF electrodes increases the normalized generated voltage from 0.37 to 1. Maximum power density happens in l_r = 44 mm ($X_{r\text{-}1}$ = 0 and X_r = 44 mm). Therefore, the tuning mechanism can enhance the output power and voltage sensitivity.

3.4 Connection configuration circuit

Fig. 6 illustrates the proposed connection configuration circuit for controlling the electrodes. The electrodes modeled by a current source in parallel with internal piezoelectric capacitance are configured by three MOSFET Switches. The optimal load resistance is determined by the equivalent piezoelectric capacitance. The amplitude of r^{th} current source is obtained by Eq. (15b) (Hadidi and Hassanzadeh 2024).

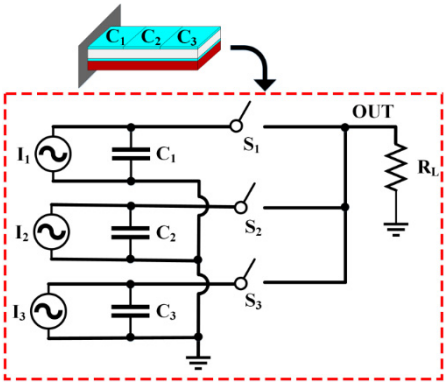

Fig. 6 Proposed connection configuration circuit

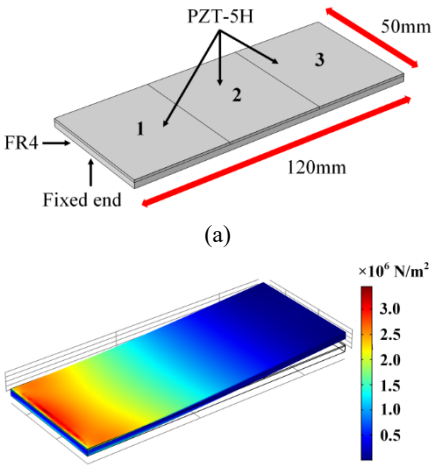

Fig. 7 Tunable piezoelectric sensor in COMSOL Multiphysics: (a) Structure; (b) Under stress

The control circuit is simulated using TSMC's 0.18 µm CMOS technology parameters, with the following assumptions: $\frac{\hbar b d_{31} \bar{F} \omega_0}{l} = I_0 = 1\ mA$, $C_1 = C_2 = C_3$ = 50 nF, and f_0 = 120 Hz. Table 1 compares the output power with the power consumption of switches in turn-on and turn-off modes. Thanks to a high d_{31} value (274 pC/N) and large switches (1000 × (2 µm/0.2 µm)), the power consumption of the switches is minimal compared to the output power.

Table 1 Power distribution in the connection configuration circuit

Switch	State	Power consumption	Output power
S_1	Turn-on	7.6 µW	835 µW
	Turn-off	68 nW	
S_2	Turn-on	826 nW	108 µW
	Turn-off	6.2 nW	
S_3	Turn-on	17 nW	4.3 µW
	Turn-off	0.9 nW	

Table 2 Mechanical properties and dimensions of the piezoelectric sensor

Properties	Materials	Symbol	Value
Young's modulus (GPa)	PZT-5H	Y	67
	FR4		22
Mass density (kg/m³)	PZT-5H	ρ	7500
	FR4		1900
Length (mm)	PZT-5H	l	120
	FR4		
Width (mm)	PZT-5H	b	50
	FR4		
Thickness (mm)	PZT-5H	h	0.5
	FR4	H	2.5

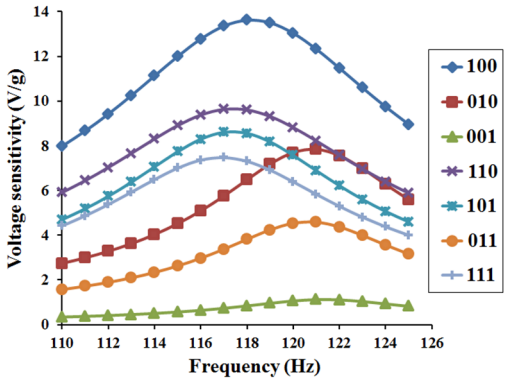

Fig. 8 Frequency response for different electrode configurations

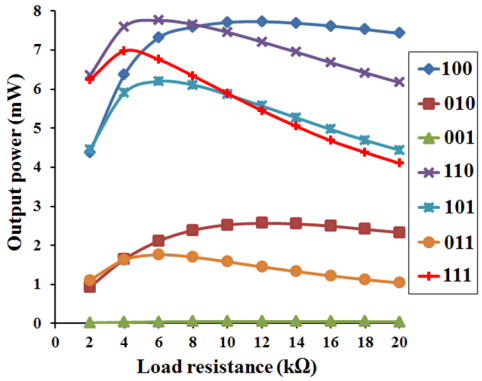

Fig. 9 Output power versus load resistance for different electrode configurations

4. Results

4.1 Simulation results

This section explores the impact of the tuning mechanism on the resonance frequency, voltage sensitivity, and output power. Fig. 7(a) shows the tunable three-segment piezoelectric sensor in the COMSOL environment. Fig. 7(b) shows the stress distribution in the cantilever beam, ranging from 0 to approximately 3.5 MPa. Table 2 provides the mechanical properties and dimensions of the proposed sensor. The frequency response for different

Table 3 Main characteristics of the vibration sensor at optimal load resistance for different electrode modes

Modes	Schematic	f_r (Hz)	-3 dB Bandwidth (Hz)	Voltage sensitivity (V/g)	Output power (mW)	$R_{L\text{-opt}}$
111	ON ON ON	116.9	111.8 - 122	7.47	6.98	4 kΩ
110	ON ON OFF	117.4	111.7 – 123.2	9.65	7.76	6 kΩ
101	ON OFF ON	117.35	112.6 – 122.1	8.67	6.2	6 kΩ
011	OFF ON ON	120.7	116.7 – 124.8	4.59	1.76	6 kΩ
100	ON OFF OFF	118.2	112.3 – 124.1	13.62	7.73	12 kΩ
010	OFF ON OFF	120.8	116.7 – 125.1	7.85	2.56	12 kΩ
001	OFF OFF ON	121.4	117.6 – 125.2	1.13	0.053	12 kΩ

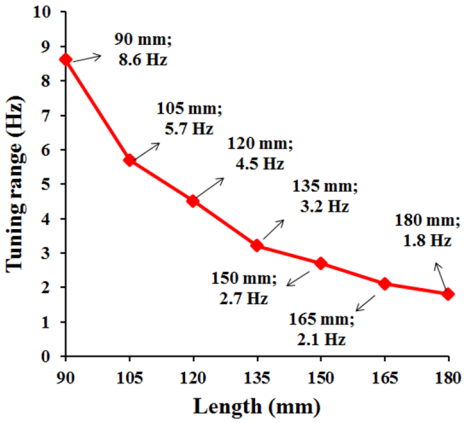

(a)

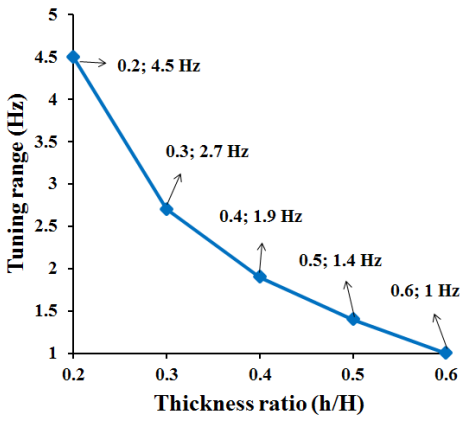

(b)

Fig. 10 Impact of length and thickness on the tuning range: (a) Length; (b) thickness ratio (h/H)

electrode configurations is shown in Fig. 8. The presented method increases the resonance frequency from 116.9 Hz to 121.4 Hz, with a tuning range of 4.5 Hz. When electrode 1 is ON (modes 111, 110, 101, and 100), the voltage sensitivity ranges from 7.47 V/g to 13.62 V/g. V/g indicates the generated voltage when the acceleration is 1 g (g = 9.8 m/s^2). Turning off electrode 1 decreases the voltage sensitivity to 4.59 V/g in mode 011, and turning simultaneously off electrode 3 increases it to 7.85 V/g in mode 010. Fig. 9 displays output power versus the load resistance for different electrode configurations. When electrode 1 is ON, the minimum output power is 6.2 mW for a 1 g input excitation level. When electrode 1 is OFF (modes 011 and 010), output power drops to the minimum of 1.76 mW. In mode 001, the output power reduces to 53 μW. In Table 3, the resonance frequency, -3 dB bandwidth, voltage sensitivity, and output power of the proposed vibration sensor for electrode modes are detailed. All modes except mode 001 exhibit high voltage sensitivity and output power. The influence of length and thickness on the tuning range is shown in Fig. 10. In Fig. 10(a), the tuning range increases from 1.8 Hz to 8.6 Hz by halving the length. Decreasing the thickness ratio from 0.6 to 0.2 increases the tuning range from 1 Hz to 4.5 Hz, as shown in Fig. 10(b). The thickness ratio is the piezoelectric thickness (h) divided by the substrate thickness (H). Therefore, split electrodes can tune the resonance frequency of the piezoelectric vibration sensor.

4.2 Experimental results

Fig. 11 illustrates the measurement setup, which includes the tunable piezoelectric sensor, a GW INSTEK AFG-2225 function generator, and a GW INSTEK GDM-8145 multimeter. Three PZT-5H piezoelectric elements are mounted on a FR4 substrate to fabricate the tunable piezoelectric sensor. Fig. 12(a) compares the resonance frequency for different electrode configurations in experimental and simulation results. In experimental and simulation results, turning off the electrodes increases the resonance frequency by about 2.5 Hz and 4.6 Hz, respectively. The error in the resonance frequency measurement in the experiment compared to simulation results is shown in Fig. 12(b). The error defined in Eq. (18) is less than 1% for all modes. Fig. 13 shows the normalized voltage sensitivity and power density for different electrode configurations in simulation and experimental results. The normalized response is obtained by dividing the output amplitude by the maximum amplitude. The maximum voltage sensitivity and power density occur in mode 100 for both simulation and experimental results, as shown in Fig. 13. The power density increases in modes 101, 110, and 100 compared to the monolithic electrode (Mode 111) in both simulation and experimental results, shown in Fig. 13(b). Turning off electrode 1 decreases the power density compared to mode 111 in simulation and experimental results. In all modes, experimental results align with

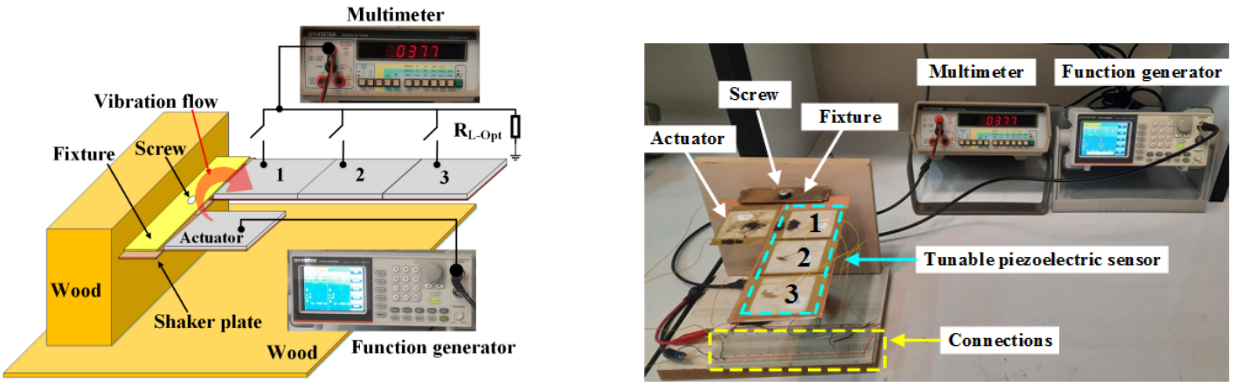

(a) (b)

Fig. 11 (a) Measurement setup; (b) schematic

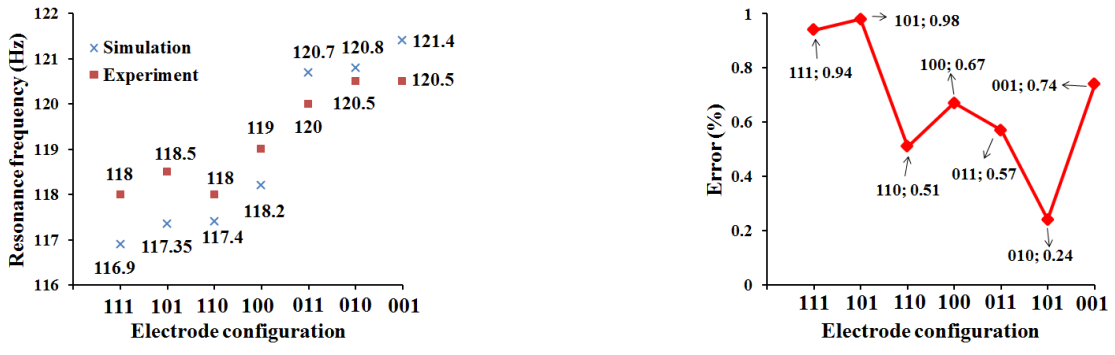

(a) (b)

Fig. 12 (a) Resonance frequency for different electrode configurations; (b) error

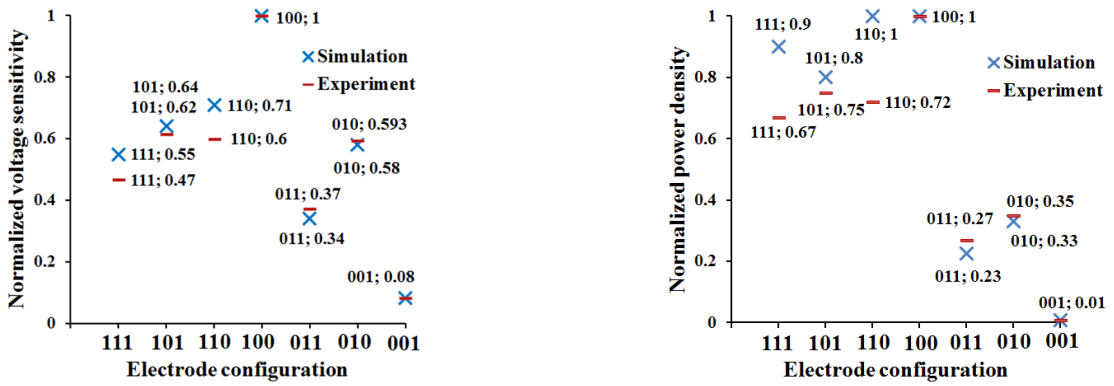

(a) (b)

Fig. 13 Normalized response for different electrode configurations: (a) Voltage sensitivity; (b) power density

Table 4 Comparison of the proposed tunable sensor with previous works

Reference	Technique	Geometric dimension	Tuning range (Hz)	Minimum power density	Maximum power density
Huet *et al*. (2022)	Mobile clamping	9.7 cm × 4.5 cm × 2.7 cm	100.8-123.1	19.18 μW/cm^{3*} (0.5 g, 31 kΩ)	401 μW/cm^{3*} (0.5 g, 26 kΩ)
Dong *et al*. (2022)	Position tuning of middle mass	-	720-725	-	-
Wang *et al*. (2021)	Sliding mass	-	6-9	-	-
Shi *et al*. (2021)	Zigzag piezoelectric springs actuated by a rolling ball	27 cm × 8 cm × 3.5 cm	1-4	-	7.5 μW/cm^{3*} (0.5 g, 5.1 kΩ)
Ganapathy *et al*. (2021)	Hybrid	-	38-54	-	-
Le Scornec *et al*. (2020)	Mobile mass	1.82 cm^2	9.9-16	94.5 μW/cm^{3*} (1 g, 280 MΩ)	166.7 μW/cm^{3*} (1 g, about 200 MΩ)
This work	Stress distribution	18 cm^3	116.9-120.8	100 μW/cm^3 (1 g, 6 kΩ)	430 μW/cm^3 (1 g, 6 kΩ)

*Calculated

simulation results. In modes 111 and 110, an acceptable error in the output voltage measurement is observed, as shown in Fig. 13(a). As illustrated in Fig. 13(b), the error in output voltage causes discrepancies in output power for modes 111 and 110. Table 4 compares the proposed tunable sensor with previous works. In Table 4, power density is calculated by dividing the output power per total device volume, including proof masses and the interface circuit. Dong *et al*. (2022), Wang *et al*. (2021), Ganapathy *et al*. (2021), and Le Scornec *et al*. (2020) present frequency-tuning mechanisms based on mass, while Ganapathy *et al*. (2021) use the magnetic effect to adjust the resonance frequency by changing the stiffness. Huet *et al*. (2022) and Shi *et al*. (2021) exploit non-conventional methods to tune the resonance frequency that severely reduces the power density. The proposed tuning mechanism fine-tunes the resonance frequency and increases the power density when electrode 1 is ON. Unlike previous works, the proposed tunable sensor does not use a magnet or an auxiliary mass and can resolve the physical uncertainty challenge of piezoelectric vibration sensors.

$$Error = \frac{|Value(Exp) - Value(Sim)|}{Value(Sim)} \times 100 \quad (18)$$

5. Conclusions

This paper proposes a self-powered tunable piezoelectric vibration sensor based on stress distribution. Unlike conventional mechanisms, the proposed tunable sensor uses split electrodes and does not need a magnetic effect or a separate mechanical system to adjust the resonance frequency. The configurable electrodes vary the stress level to change the resonance frequency. The resonance frequency changes from 116.9 Hz to 121.4 Hz. The maximum power density is 430 μW/cm^3 at 117.4 Hz, with an optimal load resistance of 6 kΩ and an input acceleration of 1 g. At 121.4 Hz, mode 001, the voltage sensitivity and power density are limited to 1.13 V/g and approximately 3 μW/cm^3, respectively, indicating minimum values within the tuning range. A length of 90 mm and a thickness ratio of 0.2 expand the tuning range up to 8.6 Hz. The new mechanism can tune the resonance frequency,

achieve self-powered functionalities, and enhance voltage sensitivity compared to the conventional sensor.

References

Al Mamun, M.A. and Yuce, M.R. (2019), "Sensors and systems for wearable environmental monitoring toward IoT-enabled applications: A review", *IEEE Sensors J.*, **19**, 7771-7788. https://doi.org/10.1109/JSEN.2019.2919352

ANSI/IEEE Std 176-1987 (1987), IEEE standard on piezoelectricity, New York: The Institute of Electrical and Electronics Engineers.

Covaci, C. and Gontean, A. (2020), "Piezoelectric energy harvesting solutions: A review", *Sensors*, **20**(12), p. 3512. https://doi.org/10.3390/s20123512

Damjanovic, D. and Demartin, M. (1996), "The Rayleigh law in piezoelectric ceramics", *J. Phys. D*: *Appl. Phys.*, **29**, p. 2057. https://doi.org/10.1088/0022-3727/29/7/046

Dong, L., Zuo, J., Wang, T., Xue, W., Wang, P., Li, J. and Yang, F. (2022), "Enhanced piezoelectric harvester for track vibration based on tunable broadband resonant methodology", *Energy*, **254**, p. 124274. https://doi.org/10.1016/j.energy.2022.124274

Du, S., Jia, Y., Chen, S.T., Zhao, C., Sun, B., Arroyo, E. and Seshia, A.A. (2017), "A new electrode design method in piezoelectric vibration energy harvesters to maximize output power", *Sensors Actuat. A*: *Phys.*, **263**, 693-701. https://doi.org/10.1016/j.sna.2017.06.026

Erturk, A. and Inman, D.J. (2008), "A distributed parameter electromechanical model for cantilevered piezoelectric energy harvesters", *J. Vib. Acoust.*, **130**, p. 041002. https://doi.org/10.1115/1.2890402

Ganapathy, S.R., Salleh, H. and Azhar, M.K.A. (2021), "Design and optimisation of magnetically-tunable hybrid piezoelectric-triboelectric energy harvester", *Scientific reports*, **11**, p. 4458. https://doi.org/10.1038/s41598-021-83776-y

Gusarov, B., Gusarova, E., Viala, B., Gimeno, L. and Cugat, O. (2016), "PVDF piezoelectric voltage coefficient in situ measurements as a function of applied stress", *J. Appl. Polym. Sci.*, **133**. https://doi.org/10.1002/app.43248

Habib, M., Lantgios, I. and Hornbostel, K. (2022), "A review of ceramic, polymer and composite piezoelectric materials", *J. Phys. D*: *Appl. Phys.*, **55**, p. 423002. https://doi.org/10.1088/1361-6463/ac8687

Hadidi, S. and Hassanzadeh, A. (2023), "A novel self-powered, high-sensitivity piezoelectric vibration sensor based on piezoelectric combo effect", *IEEE Sensors J.*, **23**(21), 25797-25803. https://doi.org/10.1109/JSEN.2023.3317445

Hadidi, S. and Hassanzadeh, A. (2024), "A high-efficiency optimized bias-flip energy harvesting system for IoT applications", *AEU-Int. J. Electron. Commun.*, **177**, p. 155197. https://doi.org/10.1016/j.aeue.2024.155197

Huet, F., Boitier, V. and Seguier, L. (2022), "Tunable piezoelectric vibration energy harvester with supercapacitors for WSN in an industrial environment", *IEEE Sensors J.*, **22**, 15373-15384. https://doi.org/10.1109/JSEN.2022.3185426

Khosravani, M.R. and Reinicke, T. (2020), "3D-printed sensors: Current progress and future challenges", *Sensors Actuat. A*: *Phys.*, **305**, p. 111916. https://doi.org/10.1016/j.sna.2020.111916

Le Scornec, J., Guiffard, B., Seveno, R. and Le Cam, V. (2020), "Frequency tunable, flexible and low cost piezoelectric micro-generator for energy harvesting", *Sensors Actuat. A*: *Phys.*, **312**, p. 112148. https://doi.org/10.1016/j.sna.2020.112148

Lee, C.K. and Moon, F.C. (1990), "Modal sensors/actuators", *Transact. ASME*, **57**, 434-441. https://doi.org/10.1115/1.2892008

Li, T. and Lee, P.S. (2022), "Piezoelectric energy harvesting technology: from materials, structures, to applications", *Small Struct.*, **3**, p. 2100128. https://doi.org/10.1002/sstr.202100128

Li, X., Teng, L., Tang, H., Chen, J., Wang, H., Liu, Y., Fu, M. and Liang, J. (2020), "ViPSN: A vibration-powered IoT platform", *IEEE Internet Things J.*, **8**, 1728-1739. https://doi.org/10.1109/JIOT.2020.3016993

Liang, H., Hao, G. and Olszewski, O.Z. (2021), "A review on vibration-based piezoelectric energy harvesting from the aspect of compliant mechanisms", *Sensors Actuat. A*: *Phys.*, **331**, p. 112743. https://doi.org/10.1016/j.sna.2021.112743

Liu, X., He, L., Liu, R., Hu, D., Zhang, L. and Cheng, G. (2023), "Piezoelectric energy harvesting systems using mechanical tuning techniques", *Rev. Scientif. Instrum.*, **94**(3), p. 031501. https://doi.org/10.1063/5.0120778

Majumder, B.D., Roy, J.K. and Padhee, S. (2018), "Recent advances in multifunctional sensing technology on a perspective of multi-sensor system: A review", *IEEE Sensors J.*, **19**, 1204-1214. https://doi.org/10.1109/JSEN.2018.2882239

Meeks, S.W. and Timme, R.W. (1975), "Effects of one-dimensional stress on piezoelectric ceramics", *J. Appl. Phys.*, **46**, 4334-4338. https://doi.org/10.1063/1.321456

Mishra, K., Panda, S.K., Kumar, V. and Dewangan, H.C. (2020), "Analytical evaluation and experimental validation of energy harvesting using low frequency band of piezoelectric bimorph actuator", *Smart Struct. Syst., Int. J.*, **26**, 391-401. https://doi.org/10.12989/sss.2020.26.3.391

Muscat, A., Bhattacharya, S. and Zhu, Y. (2022), "Electromagnetic vibrational energy harvesters: A review", *Sensors*, **22**, p. 5555. https://doi.org/10.3390/s22155555

Patel, R., McWilliam, S. and Popov, A.A. (2014), "Optimization of piezoelectric cantilever energy harvesters including non-linear effects", *Smart Mater. Struct.*, **23**, p. 085002. https://doi.org/10.1088/0964-1726/23/8/085002

Pecunia, V., Silva, S.R.P., Phillips, J.D., Artegiani, E., Romeo, A., Shim, H., Park, J., Kim, J.H., Yun, J.S., Welch, G.C. and Larson, B.W. (2023), "Roadmap on energy harvesting materials", *J. Phys.*: *Mater.*, **6**, p. 042501. https://doi.org/10.1088/2515-7639/acc550

Qin, L., Wang, J., Liu, D., Tang, L. and Song, G. (2019), "Analysis on an improved resistance tuning type multi-frequency piezoelectric spherical transducer", *Smart Struct. Syst., Int. J.*, **24**(4), 435-446. https://doi.org/10.12989/sss.2019.24.4.435

Rehman, S.U., Usman, M., Toor, M.H.Y. and Hussaini, Q.A. (2024), "Advancing structural health monitoring: A vibration-based IoT approach for remote real-time systems", *Sensors Actuat. A*: *Phys.*, **365**, p. 114863. https://doi.org/10.1016/j.sna.2023.114863

Rigo, F., Migliorini, M. and Pozzebon, A. (2024), "Piezoelectric Sensors as Energy Harvesters for Ultra Low-Power IoT Applications", *Sensors*, **24**, p. 2587. https://doi.org/10.3390/s24082587

Roundy, S., Wright, P.K. and Rabaey, J. (2003), "A study of low level vibrations as a power source for wireless sensor nodes", *Comput. Commun.*, **26**, 1131-1144. https://doi.org/10.1016/S0140-3664(02)00248-7

Shahabi, P., Ghafarirad, H. and Taghvaeipour, A. (2019), "Nonlinear vibration analysis of piezoelectric bending actuators: Theoretical and experimental studies", *Comptes Rendus Mécanique*, **347**, 953-966. https://doi.org/10.1016/j.crme.2019.10.007

Shi, G., Peng, Y., Tong, D., Chang, J., Li, Q., Wang, X., Xia, H. and Ye, Y. (2021), "An ultra-low frequency vibration energy harvester with zigzag piezoelectric spring actuated by rolling ball", *Energy Convers. Manag.*, **243**, p. 114439. https://doi.org/10.1016/j.enconman.2021.114439

Shirvanimoghaddam, M., Shirvanimoghaddam, K., Abolhasani,

M.M., Farhangi, M., Barsari, V.Z., Liu, H., Dohler, M. and Naebe, M. (2019), "Towards a green and self-powered Internet of Things using piezoelectric energy harvesting", *IEEE Access*, **7**, 94533-94556. https://doi.org/10.1109/ACCESS.2019.2928523

Sosna, P., Rubeš, O. and Hadaš, Z. (2023), "Verification and analysis of advanced tuneable nonlinear vibration energy harvester", *Mech. Syst. Signal Process.*, **189**, p. 110096. https://doi.org/10.1016/j.ymssp.2023.110096

Stewart, M., Weaver, P.M. and Cain, M. (2012), "Charge redistribution in piezoelectric energy harvesters", *Appl. Phys. Lett.*, **100**, p. 073901. https://doi.org/10.1063/1.3685701

Trentadu, F., Quaranta, G., Maruccio, C. and Marano, G.C. (2019), "Energy harvesting from piezoelectric strips attached to systems under random vibrations", *Smart Struct. Syst., Int. J.*, **24**(3), 333-343. https://doi.org/10.12989/sss.2019.24.3.333

Wang, Z., Du, Y., Li, T., Yan, Z. and Tan, T. (2021), "A flute-inspired broadband piezoelectric vibration energy harvesting device with mechanical intelligent design", *Appl. Energy*, **303**, p. 117577. https://doi.org/10.1016/j.apenergy.2021.117577

Xu, J. and Tang, J. (2015), "Linear stiffness compensation using magnetic effect to improve electro-mechanical coupling for piezoelectric energy harvesting", *Sensors Actuat. A: Phys.*, **235**, 80-94. https://doi.org/10.1016/j.sna.2015.09.026

Yan, Y., Hu, Y., Wang, L., Qian, X., Zhang, W., Reda, K., Wu, J. and Zheng, G. (2021), "Electrostatic sensors–Their principles and applications", *Measurement*, **169**, p. 108506. https://doi.org/10.1016/j.measurement.2020.108506

Yoon, H. and Youn, B.D. (2018), "System reliability analysis of piezoelectric vibration energy harvesting considering multiple safety events under physical uncertainty", *Smart Mater. Struct.*, **28**, p. 025010. https://doi.org/10.1088/1361-665X/aaf116